Grain Rotation-based Analysis Method for Shear Band

Hua-Xiang ZHU[1] and Zhen-Yu YIN[2,*]

[1] PhD, Department of Civil and Environmental Engineering, The Hong Kong Polytechnic University, Hung Hom, Kowloon, Hong Kong, China; Laboratoire Navier, CNRS, ENPC, Paris, France
[2] Associate Professor, Department of Civil and Environmental Engineering, The Hong Kong Polytechnic University, Hung Hom, Kowloon, Hong Kong, China
[*] Corresponding author: Dr. Zhen-Yu YIN, Tel: +852 3400 8470; Fax: +852 2334 6389; Email: zhenyu.yin@polyu.edu.hk; zhenyu.yin@gmail.com

Abstract: The grain rotational field is significantly associated with the shear banding process and can be derived easily on the basis of individual grains, which could be an appropriate and convenient quantity in shear band analysis. In this paper, a novel method is proposed for directly analysing the shear banding process in the granular assembly based on its grain rotational field. Numerical plain strain tests on a dense (S1) and an intermediate dense specimen (S2) are performed using the coupled Discrete Element Method (DEM) and Finite Difference Method (FDM). The grain rotational field is statistically characterised by the rotational distribution $\beta_v(\omega)$, a new index defined as the volumetric percentage of grains rotating to a greater degree than the rotation ω, in which the High Rotation (HR) section basically indicates the grains inside the shear band. A measurement of $\beta_v(\omega)$'s uniformity quantifies the degree of strain localisation, and S2 is found to perform a more uniform rotational distribution than does S1. Taking the value of ω at which $\beta_v(\omega)$'s curvature is higher than a threshold as the boundary of the HR section, HR grains are filtered out of the sample, based on which the inclination and thickness of the shear band, as well as two local quantities (average void ratio and coordination number) inside the shear band, are analysed.

Keywords: Granular materials, discrete element method, finite difference method, shear band, grain rotation, biaxial test

Introduction

The soil body subjected to shearing often deviates from homogeneity and develops patterns wherein strain appears to be localised into certain band-shaped areas known as shear bands. The soil inside the shear band is the place from which the non-elastic stress-strain behaviour primarily is derived and the zone of interest in terms of exploring the soil's mechanical properties during and after the failure. To focus on the shear band material makes more mechanical sense than to deal with the soil body as a whole. The shear band morphology, such as the inclination and thickness, and how it is related to soil's mechanical performance have been well studied in various experiments, such as those by Vardoulakis et al. (1978), Desrues et al. (1985), Vardoulakis and Graf (1985), Desrues et al. (1996) and Finno et al. (1997), as well as from theoretical viewpoints such as those of Vardoulakis et al. (1978), Petryk (1993), Tejchman and Wu (1996), Chambon and Caillerie (1999), Bigoni (2000), Sulem and Vardoulakis (2004), Tejchman and Górski (2008), Gao and Zhao (2013) and Lin et al. (2015).

Indicating the shear band from a granular assembly full of kinematic fluctuation is often the first treatment before further mechanical analyses of cases exhibiting strain localization. Various local quantities, such as the displacement, the strain, the void ratio, the force-chains and so on, are associated with the shear banding process in several studies (Oda and Kazama 1998; Alshibli and Stein 1999; Oda and Iwashita 2000; Rechenmacher 2006; Réthoré et al. 2007; Alshibli and Hasan 2008; Yin and Chang 2010; Jiang et al. 2013; Yin et al. 2014; Jiang et al. 2016). Three main complications, however, stand on the way of a rapid shear band analysis: (1) patterns in the soil could vary significantly from one case to another, or even from one state to another during the loading path; (2) the granular system normally carries a high degree of local fluctuation; and (3) such quantities as the local void ratio and strain field, although largely representative of the strain localisation, require relatively heavy

pre-processing, since they are extracted from the local kinematics (or geometry) of a cluster of particles rather than a single particle. A well-designed measurement should employ proper indicator(s) to capture all ~~possible~~ relevant patterns, disregard the local noise and be as efficient as possible. A strong association between the grain rotation and the shear banding process has been reported by both numerical studies (Bardet 1994; Oda and Kazama 1998; Kuhn 1999; Oda and Iwashita 2000; Jiang and Yin 2012) and laboratory studies (Oda et al. 1982; Mueth et al. 2000; Andò et al. 2012; Kruyt et al. 2014). Rotations probably occur when force-chains (particle clusters transmitting a larger-than-average normal force) in or around the shear band buckle under a transversal shearing (Iwashita and Oda 1998; Tordesillas 2007). On one hand, in simple terms, the rotational field localises significantly during the shear banding and coincides naturally with the localised strain; on the other, it exists at the single particle rather than at the inter-particle scale, meaning that it can be derived simply from single particles rather than from clusters (such as the strain and the void ratio). Both convenience and effectiveness can be gained when using the rotation field to analyse the shear band, making it worth a try.

In this study, shear band analyses, based on the grain rotation field, are carried out for plain strain tests using coupling between the Discrete Element Method (DEM) and Finite Difference Method (FDM). The rotational distribution $\beta_v(\omega)$ is defined as the volumetric percentage of grains rotating to a greater degree than the indicated absolute rotation ω, and through analysing $\beta_v(\omega)$ the shear band can be discriminated from the soil sample. The evolution of the degree of strain localisation, shear band inclination and width, as well as the void ratio inside the shear band, are then able to be measured accordingly. The effectiveness and efficiency of this shear band analysis will be qualified.

Material parameters and test protocol

The soil sample, modelled by DEM with linear elasticity, friction and rolling resistance, has a dimension of 70 mm × 130 mm × 16.9 mm, while being wrapped by the membrane modelled by FDM with the elastic model, as shown in Figure 1a. In particular, the rolling resistance (with a rolling friction μ_r) is assigned on each contact to mimic the interlocking effect among non-spherical soil grains (Iwashita and Oda 1998). The commercial FDM code FLAC3D 6.0 and DEM code PFC3D 5.0, developed by ITASCA Co., were employed where the coupling interface has already been provided. DEM and FDM parts interact at their interface. A set of DEM facets (3D triangle walls) are prescribed to cover surfaces of the FDM body, as vertices of these facets follow the coordinates of FDM's surface grid points on time-step basis. Contact forces from FDM to DEM are detected on each facet at the beginning of each time-step, and the retro-forces that the DEM system reacts onto the FEM (Finite Element Method) system are meanwhile transmitted to corresponding surface grid points according to the translational and rotational balance of the facets, allowing both systems to update their internal quantities (please check Documentation, FLAC3D (Fast Lagrangian Analysis of Continua) Version 6.0 for more details).

It could be highlighted that in this study the FDM only models the membrane which behaves in elastic and continuous fashion with its properties listed in Table 1. Then, four disadvantages of shaping the membrane by DEM particles could be avoided when using FDM to model membrane: (1) the modelling complexity involved in shaping the membrane by particles; (2) difficulties in applying normal stress to the membrane particles according to the surface geometry; (3) an associated but unnatural friction between the membrane and soil caused by the surface asperity of the particulate membrane; and (4) an unknown relationship between the bonding parameters among membrane particles (i.e. normal and shear stiffness) and the elastic parameters of the membrane (Young's modulus *E* and Poisson ratio *v*), which always needs a calibration.

The grain size distribution is demonstrated in Figure 1b, and some mechanical parameters are listed in Table 1. To note, instead of directly assigning normal and shear stiffness k_n and k_s to contacts, this paper adopts a scheme to relate k_n and k_s to the prescribed effective modulus E^* and stiffness ratio k_n/k_s and the geometry of two contacting objects. In this way, the uniform distribution of the elastic modulus is roughly ensured in the whole specimen (please see Documentation, FLAC3D Version 6.0 for more details about parameters). Otherwise, there is not any damping attached on particles or contacts in this study. Two samples of high (S1, initial void ratio e_0 = 0.560, containing 67707 spherical particles) and intermediate density (S2, e_0 = 0.627, containing 65428 particles) were prepared under confinement $p_0 = 100$ kPa (the minimum and maximum void ratio e_{min} and e_{max} can be reached by the modelling scheme are 0.560 and 0.743 respectively) and later compressed along the *z*-direction of rate $\dot{\varepsilon}_{zz}$ = 0.001 s^{-1} while maintaining pressure along the *x*-direction and fixing the membrane's *y*-displacement at the front and back sides.

Results and discussion

Stress and volumetric evolutions

The global deviatoric stress q (defined as $\sqrt{\frac{1}{2}}\sqrt{(\sigma_1-\sigma_2)^2+(\sigma_2-\sigma_3)^2+(\sigma_3-\sigma_1)^2}$ where σ_1, σ_2 and σ_3 are three principal stresses measured from the sample's boundary), hydrostatic stress p (defined as $\frac{\sigma_1+\sigma_2+\sigma_3}{3}$) and global void ratio e are plotted in Figure 2 with respect to the vertical strain e_{zz}. Two samples present stress hardening and softening with volumetric dilatancy and converge to similar final values of both p and q. The denser of the two reaches a higher peak stress and induces higher variation of e.

Evolution of the rotational field

At any strain state, let $\Delta\omega$ denote the incremental grain rotation field during a small deformation increment ($\Delta\varepsilon_{zz}$ = 0.05%). We can summarise this field via the rotational

distribution $\beta_v(\omega)$, which is the volumetric (or, say, mass) percentage of grains rotating to a greater degree than indicated by ω, so that $\beta_v(0.0) \equiv 1.0$ and $\beta_v(\infty) \equiv 0.0$. Some critical strain states of S1 are considered in Figure 3 with their $\beta_v(\omega)$, compared with those of S2 in Figure 4. Each presented curve composes roughly three sections: the Low Rotational (LR) section, containing a sharply quasi-linear decrease of β_v and a majority of grains performing a low degree of rotation; the High Rotational (HR) section, featuring a mildly quasi-linear decrease and a small portion of grains with high rotation; and the Transmission (TM) section, linking two former sections, where β_v shows a highly non-linear reduction. The way to a persistent shear band corresponds to the rotation vanishing in the LR section and increasing in the HR section because the rotational movement gradually diminishes outside the shear band and concentrates into it. During the shear banding process, therefore, the LR, HR and TM sections become automatically associated with the outside and inside shear band areas and the transition area respectively, and $\beta_v(\omega)$ evolves towards an increasing non-uniformity. Basically, a lower uniformity of $\beta_v(\omega)$ indicates a more thorough localisation of local kinematics, and therefore the degree of strain localisation can be evaluated via measuring $\beta_v(\omega)$'s uniformity.

In light of the method of quantifying the uniformity of the Grain Size Distribution, i.e. the uniformity coefficient $c_u = D_{60}/D_{10}$ (D_x denotes the grain diameter of x% passing weight), we here introduce the uniformity coefficient as the ratio of a rotation in the high rotational group over one in the lower rotational group. Assuming that ω_x is the rotation of x% passing volume, evolutions of ω_{10}, ω_{30} and ω_{50} are plotted in Figure 5. Considering the fact that $\omega_{x\geq 50}$ normally vanishes after the formation of a steady shear band for most cases, ω_{30}/ω_{10} could sensibly indicate the extent to which a rotation field has localised. The results shown in Figure 6 demonstrate that, in both samples, a consistently descending rotational uniformity (i.e. rising rotational localisation) was present before reaching steady states. S2

(the intermediate sample) always constitutes the rotational field in a more uniform manner than does S1 (the dense one). It is worthy of noting that ω_{30}/ω_{10} could become less indicative after the formation of shear band for cases in which the shear band holds a very small fraction of the specimen volume that ω_{30} is inappreciable, such as what sometimes happen in the specimen containing a large number of particles. In these cases, alternatives, such as ω_{20}/ω_{10} or ω_{10}/ω_{5}, could be considered.

Shear band parameters

After sufficient shear deformation, because the rotation magnitude diverges from the interior to the exterior shear band, it provides a chance for a direct method of filtering shear band grains for further shear band analyses. The basic idea is to separate from the entire rotational spectrum the HR section that is largely indicative of shear band grains.

Shear band direction, width and void ratio

After plotting the curvature k of $\beta_v(\omega)$, the first place where k passes 1.0, searched reversely along the ω axis, is considered here as the onset of the HR section (denoted as ω_{HR}), as shown in Figure 7 (for states ε_{zz} = 15.0%). Grains of $\omega \geq \omega_{\mathrm{HR}}$, which are plotted in Figure 8, are found to be crowded inside diagonal bands and infrequent outside them. To a remarkable extent, the chosen grains spatially follow the shear band areas and succeed in sketching the patterns.

Considering that on x - z plane, the signed distance d_i from a point i (x_i, z_i) to a line (taking the form $\mathrm{ax} - \mathrm{z} + \mathrm{b} = 0$) is equal to $(\mathrm{ax}_i - \mathrm{z}_i + \mathrm{b})/\sqrt{a^2 + 1}$, the axis of the shear band should minimise $\sum_i^{N_g} d_i^2$, where N_g is the number of considered grains. After the axis of the shear band was determined, the distribution of d was plotted in Figure 9. The 10$^{\mathrm{th}}$ and 90$^{\mathrm{th}}$ percentiles of the distribution of d are regarded as lower and upper shear band bounds respectively (two bold vertical lines in Figure 9a and 9b), and the thickness (or width) of shear band is the distance from lower to upper bound. In other words, 20% grains that were

178 furthest from the axis (10% from the left and right respectively) were excluded from the
179 defined shear band. The principal and thickness of the shear bands are demonstrated in Figure
180 10.

181 If we define all HR grains as shear band grains and the remainder as outside shear
182 bands, shear band (implied by the mark *sb*) and outside shear band (implied by *osb*)
183 quantities, plotted in Figure 11, are measured by setting measurement spheres, of radius $4D_{50}$,
184 centring at the centroids of sampled *sb* (or *osb*) grains: average void ratio *e* and average
185 coordinate number Z, which is the average number of contacts per grain in the considered
186 region.

187 Average void ratios *e* in *sb* domains of two specimens diverge from their *osb* values
188 from the early stages of the loading and converge at similar final values at large deformations.
189 *Sb* domains undergo a significantly larger dilatancy than do *osb* domains. Similar patterns
190 exist for evolutions of average coordinate number Z, where we see a convergence of *sb* Z in
191 both specimens and a larger Z of *sb* than *osb* domains.

192 *Other possible criteria for* ω_{HR}

193 So far, we have regarded the value of ω where $k = 1$ is the criterion for filtering the
194 HR grains, i.e. $\omega_{HR} = \omega|_{k=1}$. Other criteria are also discussable for ω_{HR}. A possible
195 threshold for the HR section is the mean rotation $\bar{\omega}$, i.e. $\omega_{\mathrm{HR}} = \bar{\omega}$. Three criteria, ω_{HR} being
196 equal to $\omega|_{k=1}$, $\omega|_{k=2}$ or $\bar{\omega}$, are compared in Figure 12. At steady phases (around $\varepsilon_{zz} > 6\%$
197 according to Figure 2), for both samples, three criteria (especially $\omega|_{k=1}$ and $\bar{\omega}$) yield similar
198 volumes of HR grains. In other words, $\omega_{\mathrm{HR}} = \bar{\omega}$ could be another criterion fair enough to
199 filter the HR grains, compared with $\omega_{HR} = \omega|_{k=1}$ and $\omega_{HR} = \omega|_{k=2}$. It would be a great
200 convenience to the shear band analysis that $\bar{\omega}$ could be the bound of HR grains. However,
201 further research should be incorporated to examine whether $\omega_{\mathrm{HR}} = \bar{\omega}$ is as appropriate for

most of soil samples as the criteria referring to curvature, such as $\omega_{HR} = \omega|_{k=1}$, after the formation of the shear band.

Conclusions

After plain strain tests for a dense and an intermediate specimen using coupled FDM and DEM, shear band analyses were conducted based on the grain rotational field.

The rotational distribution $\beta_v(\omega)$, a novel quantity defined as the volumetric percentage of grains rotating beyond an indicated rotation ω, was proposed to statistically characterise the grain rotational field. $\beta_v(\omega)$, which is naturally composed of LR, HR and TM sections, and the HR section basically indicated grains inside the shear band. The degree of strain localisation was indicated by measuring $\beta_v(\omega)$'s uniformity, as S1 performed a lower uniformity of $\beta_v(\omega)$ than S2.

Taking the value of ω at which $\beta_v(\omega)$'s curvature was k = 1 as the boundary of the HR section, the HR grains were selected out of the sample. According to the positions of HR grains, we calculated the inclination and thickness of the shear band. Through setting measurement sphere centring at sampled grains, two local quantities (average void ratio and coordinate number) inside the shear band were measured and compared with those obtained outside it. Tested local quantities showed remarkable divergence between the inside and outside shear bands; however, convergent values were developed inside the shear bands of two specimens. The shear band area featured a higher void ratio and a lower coordinate number.

Acknowledgments

The financial support for this research came from the National Natural Science Foundation of China (No. 51579179).

References

Alshibli, K. A., and Hasan, A. (2008). "Spatial variation of void ratio and shear band thickness in sand using X-ray computed tomography." *Géotechnique*, 58(4), 249–257.

Alshibli Khalid A., and Sture Stein. (1999). "Sand Shear Band Thickness Measurements by Digital Imaging Techniques." *Journal of Computing in Civil Engineering*, 13(2), 103–109.

Bardet, J. P. (1994). "Observations on the effects of particle rotations on the failure of idealized granular materials." *Mechanics of materials*, 18(2), 159–182.

Bigoni, D. (2000). *Bifurcation and instability of non-associative elastoplastic solids*. Springer.

Chambon, R., and Caillerie, D. (1999). "Existence and uniqueness theorems for boundaryvalue problems involving incrementally non linear models." *International journal of solids and structures*, 36(33), 5089–5099.

Desrues, J., Chambon, R., Mokni, M., and Mazerolle, F. (1996). "Void ratio evolution inside shear bands in triaxial sand specimens studied by computed tomography." *Géotechnique*, 46(3), 529–546.

Desrues, J., Lanier, J., and Stutz, P. (1985). "Localization of the deformation in tests on sand sample." *Engineering Fracture Mechanics*, 21(4), 909–921.

Finno, R. J., Harris, W. W., Mooney, M. A., and Viggiani, G. (1997). "Shear bands in plane strain compression of loose sand." *Geotechnique*, 47(1), 149–165.

Gao, Z., and Zhao, J. (2013). "Strain localization and fabric evolution in sand." *International Journal of Solids and Structures*, 50(22), 3634–3648.

Iwashita, K., and Oda, M. (1998). "Rolling resistance at contacts in simulation of shear band development by DEM." *Journal of engineering mechanics*, 124(3), 285–292.

Jiang, M.J., Liu, J.D., Sun, Y.G., Yin, Z.-Y. (2013). "Investigation into macroscopic and microscopic behaviors of bonded sands using the discrete element method." Soils and Foundations, 53: 804-819.

Jiang, M.J. and Yin, Z.-Y. (2012). "Analysis of stress redistribution in soil and earth pressure on tunnel lining by discrete element method." Tunnelling and Underground Space Technology, 32: 251-259.

Jiang, M.J., Yin, Z.-Y., Shen, Z.F. (2016). "Shear band formation in lunar regolith by discrete element analyses." Granular matter, 18: 32.

Kuhn, M. R. (1999). "Structured deformation in granular materials." *Mechanics of materials*, 31(6), 407–429.

Lin, J., Wu, W., and Borja, R. I. (2015). "Micropolar hypoplasticity for persistent shear band in heterogeneous granular materials." *Computer Methods in Applied Mechanics and Engineering*, 289, 24–43.

Oda, M., and Iwashita, K. (2000). "Study on couple stress and shear band development in granular media based on numerical simulation analyses." *International Journal of Engineering Science*, 38(15), 1713–1740.

Oda, M., and Kazama, H. (1998). "Microstructure of shear bands and its relation to the mechanisms of dilatancy and failure of dense granular soils." *Geotechnique*, 48(4), 465–481.

Petryk, H. (1993). *Theory of bifurcation and instability in time-independent plasticity*. Springer.

Rechenmacher, A. L. (2006). "Grain-scale processes governing shear band initiation and evolution in sands." *Journal of the Mechanics and Physics of Solids*, 54(1), 22–45.

Réthoré, J., Hild, F., and Roux, S. (2007). "Shear-band capturing using a multiscale extended digital image correlation technique." *Computer Methods in Applied Mechanics and Engineering*, 196(49), 5016–5030.

Sulem, J., and Vardoulakis, I. G. (2004). *Bifurcation analysis in geomechanics*. CRC Press.

Tejchman, J., and Górski, J. (2008). "Deterministic and statistical size effect during shearing of granular layer within a micro-polar hypoplasticity." *International journal for numerical and analytical methods in geomechanics*, 32(1), 81–107.

Tejchman, J., and Wu, W. (1996). "Numerical simulation of shear band formation with a hypoplastic constitutive model." *Computers and Geotechnics*, 18(1), 71–84.

Tordesillas, A. (2007). "Force chain buckling, unjamming transitions and shear banding in dense granular assemblies." *Philosophical Magazine*, 87(32), 4987–5016.

Vardoulakis, I., Goldscheider, M., and Gudehus, G. (1978). "Formation of shear bands in sand bodies as a bifurcation problem." *International Journal for numerical and analytical methods in Geomechanics*, 2(2), 99–128.

Vardoulakis, I., and Graf, B. (1985). "Calibration of constitutive models for granular materials using data from biaxial experiments." *Géotechnique*, 35(3), 299–317.

Yin, Z.-Y.; Chang, C.S. and Hicher, P.Y. (2010). "Micromechanical modelling for effect of inherent anisotropy on cyclic behaviour of sand." International Journal of Solids and Structures, 47(14-15): 1933-1951.

Yin, Z.-Y.; Zhao, J. and Hicher, P.Y. (2014). "A micromechanics-based model for sand-silt mixtures." International Journal of Solids and Structures, 51(6): 1350–1363.

Tables

Table 1. Material parameters

DEM set						FDM set		
effective modulus E^* (MPa)	Normal to shear stiffness ratio k_n/k_s	Rolling friction μ_r	Ball-ball friction μ_{b-b}	Ball-membrane friction μ_{b-m}	Particle density (kg/m^3)	Membrane thickness t_m	Young's modulus E (MPa)	Poisson's ratio v
500	2.5	0.1	0.4	`0.2	2650	0.2	3.0	0.5

Figure captions

Fig. 1. (a) Setup of the model and (b) grain size distribution.

Fig. 2. (a) Deviatoric stress q and (b) void ratio e with respect to vertical strain ε_{zz}.

Fig. 3. Volumetric percentage β_v of grains rotating beyond ω at several strain states ($\Delta\varepsilon_{zz}$ = 2.0% occurs around the peak stress).

Fig. 4. For samples S1 and S2, volumetric percentage β_v of grains rotating beyond ω at several strain states ($\Delta\varepsilon_{zz}$ = 2.0% occurs around the peak stress).

Fig. 5. ω_{10}, ω_{30} and ω_{50} with respect to ε_{zz} for sample S1 and S2.

Fig. 6. ω_{30}/ω_{10} with respect to ε_{zz} for sample S1 and S2.

Fig. 7. Volumetric percentage β_v (black line) of grains rotating beyond ω and curvature k (red line) at ε_{zz} = 15.0% for (a) S1 and (b) S2.

Fig. 8. Grains rotating more than ω_{HR} at ε_{zz} = 15.0% in (a) S1 and (b) S2.

Fig. 9. For (a) S1 and (b) S2 at ε_{zz} = 15.0%, probability density of d and the percentile box, on which five vertical lines denote 10$^{\mathrm{th}}$ (black), 25$^{\mathrm{th}}$ (grey), 50$^{\mathrm{th}}$ (grey), 75$^{\mathrm{th}}$ (grey) and 90$^{\mathrm{th}}$ (black) percentile respectively.

Fig. 10. Centroids of grains rotating more than ω_{HR} (grey points) and measured axis and width of shear band at ε_{zz} = 15.0% for (a) S1 and (b) S2.

Fig. 11. In terms of ε_{zz} for S1 and S2, average void ratio e and average coordinate number Z inside (*sb*) and outside shear band (*osb*).

Fig. 12. With respect to ε_{zz}, evolutions of $\beta_v|\omega = \omega_{\mathrm{HR}}$ at ω_{HR} determined by several criteria for (a) S1 and (b) S2.

Figure 2

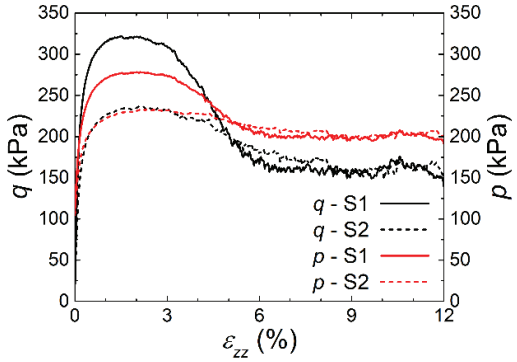

(a)

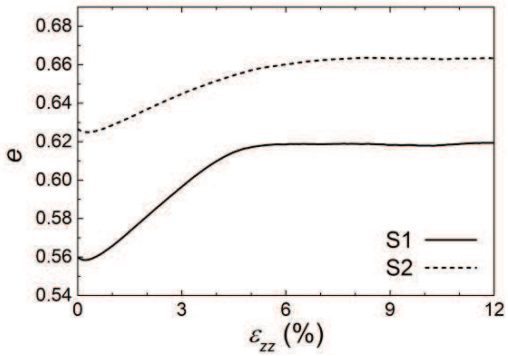

(b)

Figure 3

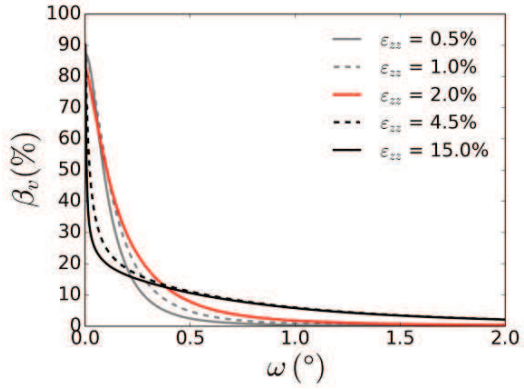

Figure 4

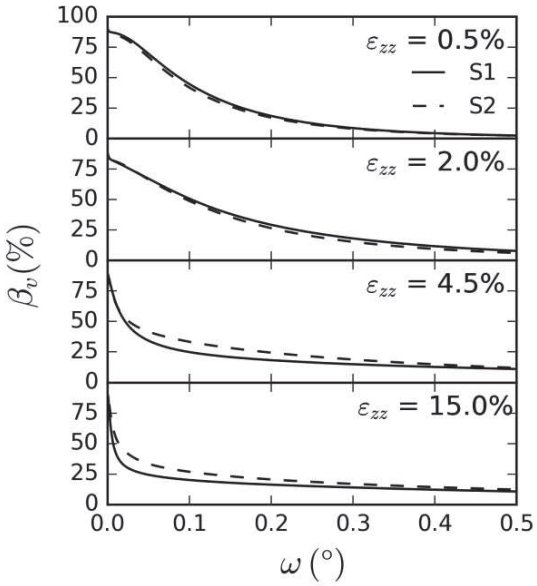

Figure 5

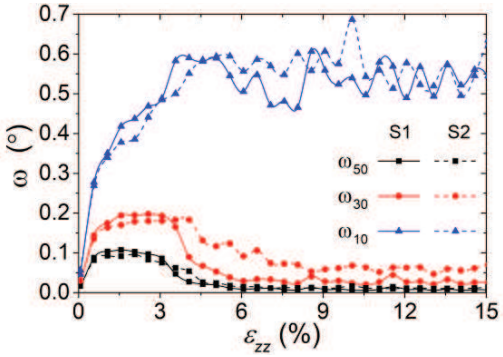

Figure 6

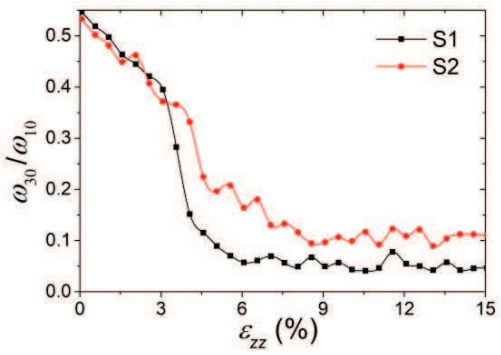

Figure 7

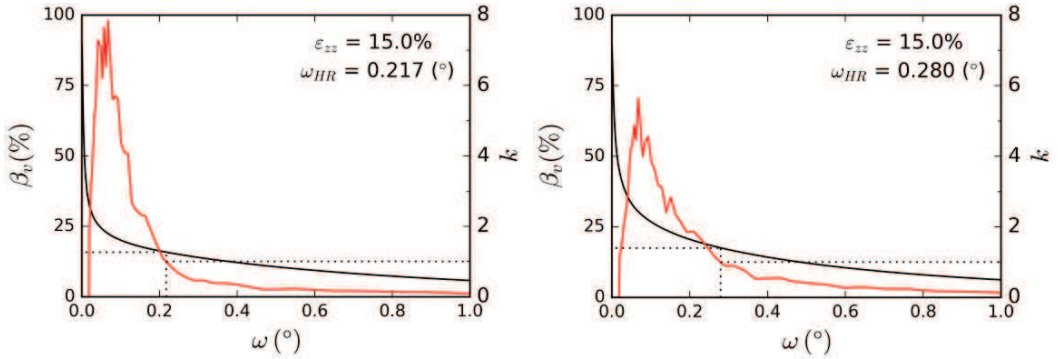

(a) (b)

Figure 8

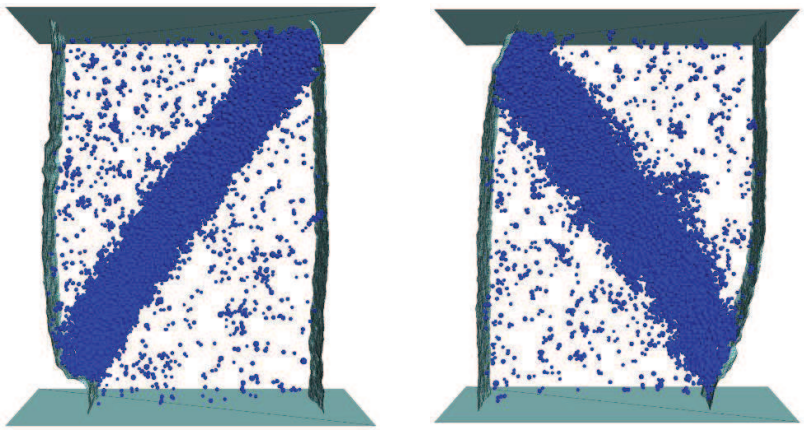

(a) (b)

Figure 9

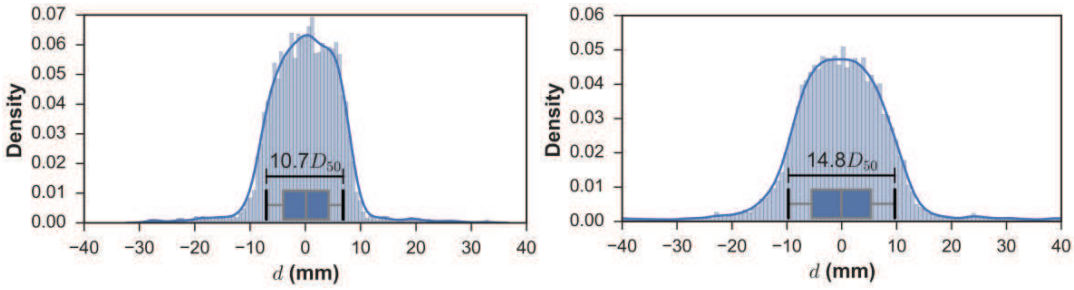

(a) (b)

Figure 10

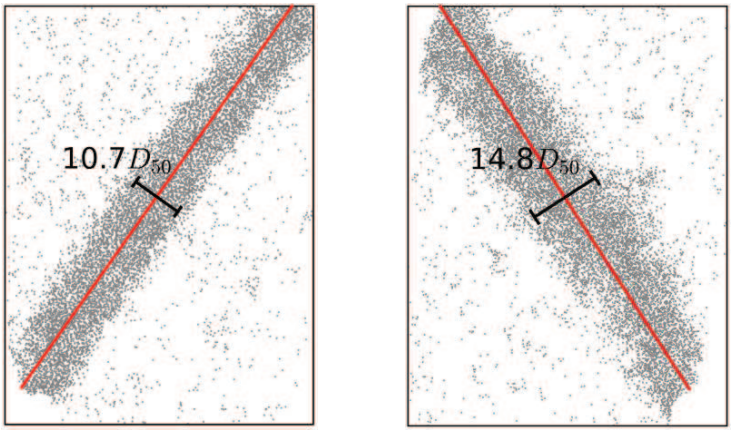

(a) (b)

Figure 11

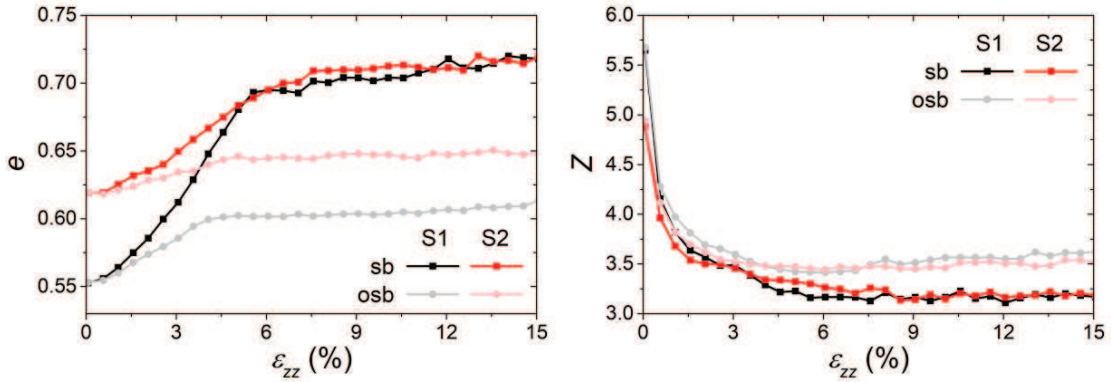

(a) (b)

Figure 12

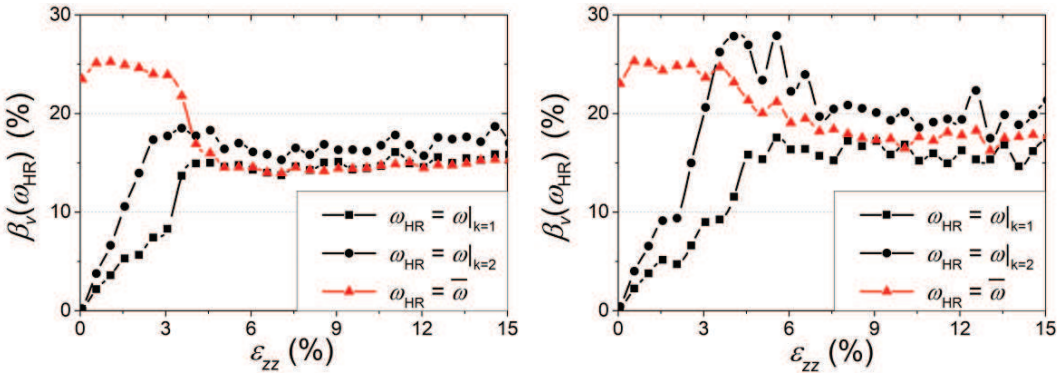

(a) (b)

Figure 1

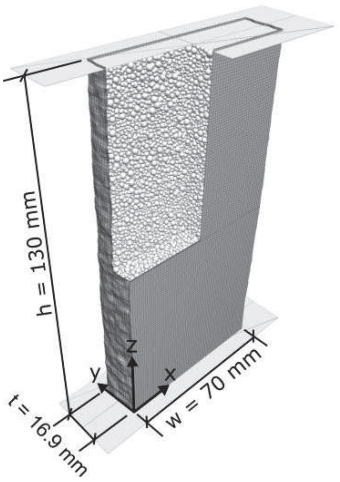

(a)

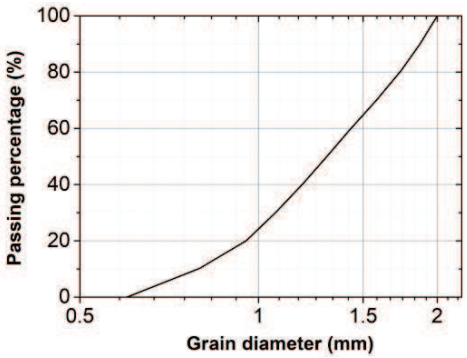

(b)